Journal of Molecular Modeling (2019) 25: 189
https://doi.org/10.1007/s00894-019-4070-z

ORIGINAL PAPER

# A computational study on the characteristics of open-shell H-bonding interaction between carbamic acid ($NH_2COOH$) and $HO_2$, HOS or HSO radicals

Adnan Ali Khan [1,2] · Mehdi D. Esrafili [3] · Aziz Ahmad [4] · Emily Hull [5] · Rashid Ahmad [1,2] · Saeed Ullah Jan [1,2] · Iftikhar Ahmad [1,6]

Received: 1 March 2019 / Accepted: 22 May 2019 / Published online: 14 June 2019


## Abstract

Quantum chemical computations were applied to investigate the characteristics of open-shell hydrogen-bonding interactions in the complexes of carbamic acid ($NH_2COOH$, CA) with $HO_2$, HOS and HSO radicals. All the resulting complexes were studied using the MP2, B3PW91 and B3LYP computational levels and 6311++G** basis set. Geometry optimizations show that the O–H···O contact is stronger than N–H···O and S–H···O. The interaction energies revealed that all the radicals form stronger hydrogen bonded complexes at site-1, as confirmed by electron-density ($\rho$) and corresponding Laplacian ($\nabla^2\rho$) values obtained by atoms in molecule (AIM) analysis. Non-covalent interaction and reduced density gradient analysis support the AIM results. Natural bond orbital analysis was employed to obtain the stabilization energies ($E^{(2)}$) due to charge delocalization between the interacting units. Energy decomposition analysis suggests that, for the title complexes, the exchange energy makes a larger contribution to the total interaction energy compared to other energy terms.

**Keywords** Opened-shell hydrogen bonding · Ab initio · Radical · DFT · MP2

## Introduction

The role of radicals in the atmosphere is really important because of their contribution to the creation of environmental problems, e.g., climatic change, air pollution, acid rain, and aerosols [1–3].In this regard, the hydroxyl peroxy ($HO_2$) and thioperoxy (HSO, HOS) radicals are among the most important moieties playing a dominant role in the atmospheric pollution [1, 4, 5]. $HO_2$ forms by the interaction of OH radicals with CO in non-polluted areas at low $NO_x$ concentrations (>10 ppb) [2, 6].

$$OH + CO \rightarrow H + CO_2 \quad (1)$$

$$H + O_2 \rightarrow HO_2 \quad (2)$$

$HO_2$ radicals further interact with $O_3$, which results in the formation of OH radicals. Hydrogen-peroxide generated by the reaction of $HO_2$-radicals is a main source of ozone-depletion and plays an important role in stratospheric and tropospheric oxidation reactions [8–12]. On the other hand, thioperoxy radicals (HOS and HSO) are simple isomeric radicals representative of many sulfur oxo-acids with the composition -[Hx,Sy,Oz], and are of particular interest as potential intermediates in the catalytic depletion of ozone:

$$HS + O_3 \rightarrow HSO + O_2 \quad (3)$$

$$HSO + O_3 \rightarrow HS + 2O_2 \quad (4)$$

**Electronic supplementary material** The online version of this article (https://doi.org/10.1007/s00894-019-4070-z) contains supplementary material, which is available to authorized users.

✉ Rashid Ahmad
rashmad@gmail.com

1 Center for Computational Materials Science, University of Malakand, Chakdara, Khyber Pakhtunkhwa, Pakistan

2 Department of Chemistry, University of Malakand, Chakdara, Khyber Pakhtunkhwa, Pakistan

3 Department of Chemistry, Faculty of Basic Science, University of Maragheh, Maragheh P.O. Box 55136-553, Iran

4 CAS Key Laboratory of Carbon Materials, Institute of Coal Chemistry, Taiyuan, People's Republic of China

5 Eurofins Lancaster Laboratories, PSS 2425 New Holland Pike, Lancaster, PA 17601, USA

6 Department of Physics, Abbottabad University of Science and Technology, Havelian, Khyber Pakhtunkhwa, Pakistan

In episulfide oxidations, $H_2S$ and the organic-thiols HSO and HOS are intermediates that feed in to the global geobiochemical sulfur cycle and air pollution [4, 5, 13]. There are many reports in the literature on the chemistry of these radicals in the atmosphere [1–15]. Hydrogen bonding (HB) is a very significant concept because it can enhance the stability of a radical that migrates far away from its site of generation, and HB can change kinetic behavior by increasing the lifetime of distant molecules [8]. Therefore, literature reports describe many HB-systems, including the combination of $SO_3$, HCl, $H_2O$, $NH_3$, $H_2SO_4$ and $CH_3X$ (X = halogens) with $HO_2$ radical, and closed or opened-shell HB interactions between HNO and $HO_2$, HCO radicals [16–22]. The open-shell intermolecular HB of HSO and $HO_2$ radicals was initially reported with formaldehyde and formic-acid, and an SH···O blue-shifted HB was identified [23]. Researchers are trying to design various materials for the sequestration of pollutants from the environment, e.g., by loading different organic molecules onto the surfaces of nano materials to tune their sensing properties towards various pollutants, i.e., gases and metals [24–26]. Therefore, an understanding of the intermolecular interactions of these organic molecules with various pollutants is really significant for the improved design of such materials.

Carbamic acid ($NH_2COOH$, CA) plays an important role in synthetic and environmental chemistry because of the existence of two protons donors (O–H and N–H) and one acceptor site (C=O) [27]. This molecule is therefor expected to form open-shell HB (OSHB) complexes with $HO_2$, HSO and HOS radicals via three different sites. Analysis of radical–carbamic acid OSHB interactions (HOO···CA, HSO···CA and HOS···CA) may contribute to better interpretation of environmental and synthetic chemistry.

## Computational methods

All computations were performed by means of Gaussian-09 software [28]. The geometries of monomers and all complexes were minimized using the opt = verytight option at the unrestricted B3LYP [29], B3PW91 [30] and MP-2 [31] methods by employing standard basis set (6-311++G (d,p)) [32]. A doublet spin state was considered for the OOH, HOS and HSO radicals and their complexes with CA. The nature of all optimized structures was confirmed by performing vibration frequency computations at the B3LYP /6-311++G (d,p) and MP-2/6-311++G (d,p) levels. No imaginary frequency was found for minimized structures, so they are local minima on the corresponding energy surface. Figure 1 represents the structure of an isolated carbamic acid (CA) molecule, indicating sites (S-1, S-2, S-3) where HOO, HOS and HSO radicals are attached for analyzing OSHB. We investigated nine types of complex of CA with HOO, HOS and HSO radical: CA···$HO_2$(S-1), CA···$HO_2$(S-2), CA···$HO_2$(S-3), CA···HSO(S-1), CA···HSO(S-2), CA···HSO(S-3), CA···HOS(S-1), CA···HOS(S-2) and CA···HOS(S-3) (S-1, S-2 and S-3 in parentheses show the attachment of radicals via three different sites of CA). The HB energies ($\Delta E_{int}$) were evaluated by subtracting the total energy of the monomers from the total energy of the complex. All $\Delta E_{int}$ were corrected for basis set superposition error (BSSE) by applying counterpoise (CP) correction [33]. The Truhlar scheme [34] was used for extrapolation of the MP-2/CBS limit by using aug-cc-pVDZ and aug-cc-pVTZ basis sets for both MP2 interaction energies and BSSE. The values used for "alpha" and "beta" were taken from Zhao and Truhlar [35]. The LMOEDA method [36, 37] was used for energy decomposition analysis (EDA) as implemented in the GAMESS US [38, 39] package using the MP2/aug-ccpVDZ method. By performing EDA analysis, the total $\Delta E_{int}$ of each complex was decomposed into electrostatic (ES), repulsion (REP), exchange (EX), dispersion (DISP) and polarization (POL) components.

$$E_{tot} = ES + EX + REP + POL + DISP \quad (5)$$

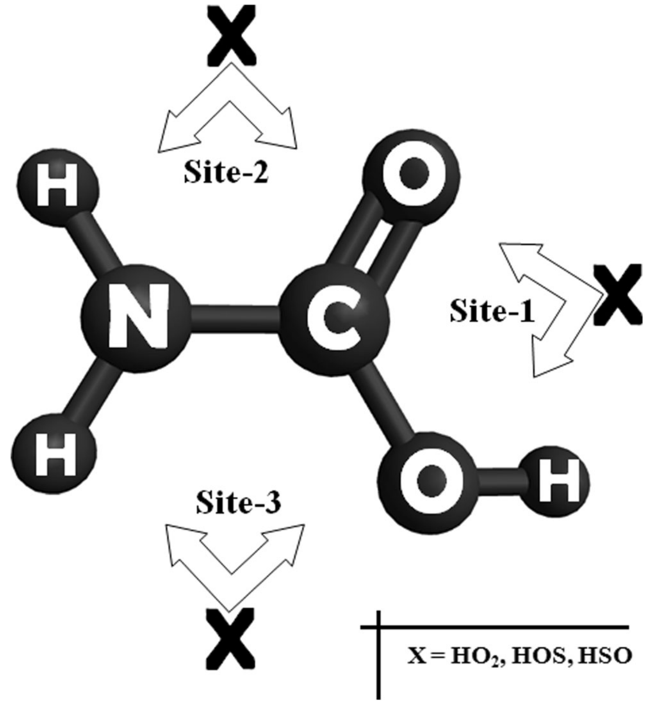

**Fig. 1** Schematic representation of different sites of carbamic acid (CA). *Arrows* Sites (S-1, S-2, S-3) where HOO, HOS and HSO radicals are attached

## Results and discussion

### Molecular electrostatic potentials, optimized structures and interaction energies

To obtain insight into the reactivity of a molecule, it is necessary to understand the electrostatic and energetic character of its appropriate known surfaces. Therefore, we computed the

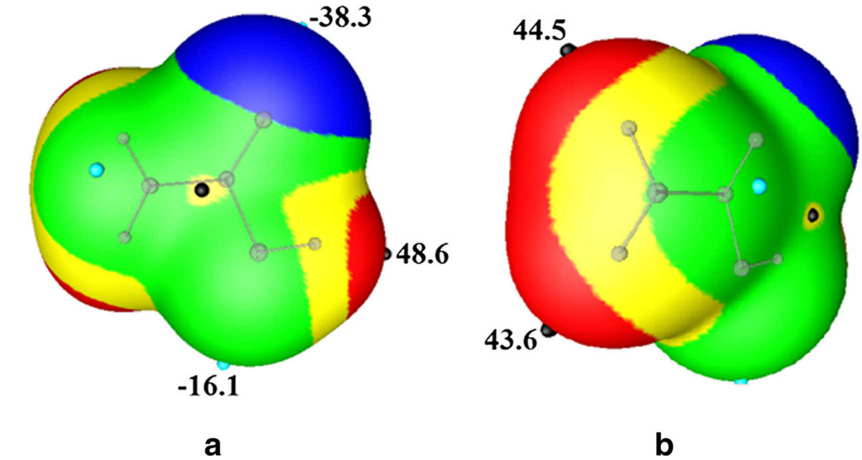


**Fig. 2** **a**,**b** Computed molecular electrostatic potential (MEP) at the 0.001 electrons/Bohr$^3$ contour of CA. **a** Front view. **b** Back view. The *black sphere* on the *red region* (positive region) shows the most positive region, and the *light blue sphere* on the *dark blue region* (negative region) shows the most negative region. Values are in kcal mol$^{-1}$

electrostatic-potential-maxima and minima ($V_{\text{s-max}}$ and $V_{\text{s-min}}$) of the CA using the WFA-SAS program [S9]. With the help of the plotted electrostatic potential map shown in Fig. 2, three sites (S-1, S-2 and S-3) were identified for the intermolecular interaction of CA with $HO_2$, HSO and HOS radicals. As seen, there are three electron-deficient and two electron-rich regions on the surface of CA. The molecular electrostatic potential (MEP) values for S-1, S-2 and S-3 are 48.6, 44.5 and 43.6 kcal mol$^{-1}$, respectively, while the values of $V_{\text{s-min}}$ for S-1 are −38.3 and S-3 is −16.1 kcal mol$^{-1}$. The MEPs values propose that S-1 is the more-favorable site to interact with the title radicals as compared to S-2 and S-3.

The optimized structures of monomers and complexes of CA with HOO, HOS and HSO radicals are shown in Fig. 3. All the HB complexes are open-shell systems. The types of HB interaction via the three different sites are XH⋯Y and Y⋯HX (X = O, S and N and Y = O and S). As shown in Fig. 3, all the H-bonded complexes of CA with HOO, HOS and HSO radicals form cyclic structures consist of seven-member rings. The bond lengths are listed in Table 1. The O–H and N–H bond lengths were found to elongate in the complexes, suggesting red-shifted HB. On the other hand, S–H bond lengths decreased upon complex formation, indicating blue-shifted HB in CA⋯HSO complexes at S-1, S-2 and S-3. Note that the amount of O–H bond elongation in HOS complexes is smaller than that in $HO_2$ complexes. The calculated HB distances in the complexes are as follows: in CA⋯OH(S-1): O–H⋯O, O⋯H–O are 1.764, 1.599 Å; in CA⋯HSO(S-1): O–H⋯O, O⋯H–S are 1.756, 2.002; in CA⋯OH(S-2): N–H⋯O, O–H⋯O are 2.031, 1.658 Å; in

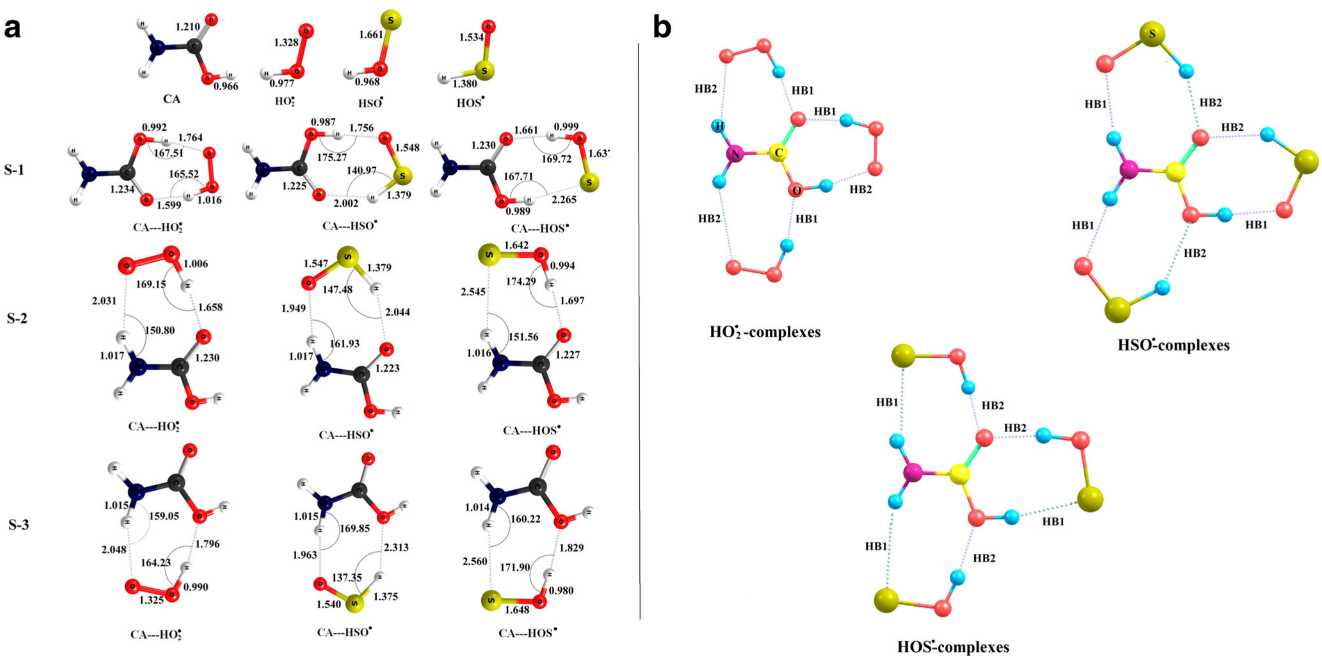


**Fig. 3** **a** Optimized geometries of open shell H-bonded (OSHB) complexes obtained at B3LYP/6–311++G** level in S-1, S-2 and S-3. **b** Key for HBs on S1, S2 and S3 sites

**Table 1** Optimized geometrical parameters bond lengths (Å) and angles (°) computed at various levels of theories and 6–311++G(d,p) basis set

| Complex | Method | HB1[a] | HB2[a] | ∠1 | ∠2 | O–$H_a$[b,d] | O–$H_b$[c,d] | N–H | S–H |
|---|---|---|---|---|---|---|---|---|---|
| CA···$HO_2$(S1) | B3LYP | 1.599 | 1.764 | 166 | 168 | 0.992 | 1.016 | | |
| | B3PW91 | 1.561 | 1.713 | 166 | 168 | 0.995 | 1.021 | | |
| | MP2 | 1.603 | 1.752 | | | 0.987 | 1.007 | | |
| CA···$HO_2$(S2) | B3LYP | 1.658 | 2.031 | 169 | 151 | | 1.006 | 1.017 | |
| | B3PW91 | 1.630 | 1.997 | 170 | 151 | | 1.008 | 1.017 | |
| | MP2 | 1.674 | 2.068 | 169 | 150 | | 0.995 | 1.013 | |
| CA···$HO_2$(S3) | B3LYP | 1.796 | 2.048 | 164 | 159 | | 0.990 | 1.015 | |
| | B3PW91 | 1.783 | 2.031 | 164 | 159 | | 0.989 | 1.014 | |
| | MP2 | 1.813 | 2.091 | 164 | 159 | | 0.982 | 1.012 | |
| CA···HSO(S1) | B3LYP | 1.756 | 2.002 | 175 | 141 | 0.987 | | | 1.379 |
| | B3PW91 | 1.727 | 1.948 | 176 | 142 | 0.988 | | | 1.381 |
| | MP2 | 1.658 | 2.057 | 176 | 134 | 0.991 | | | 1.363 |
| CA···HSO(S2) | B3LYP | 1.949 | 2.044 | 162 | 147 | | | 1.017 | 1.379 |
| | B3PW91 | 1.931 | 2.002 | 163 | 149 | | | 1.017 | 1.381 |
| | MP2 | 1.861 | 2.111 | 162 | 139 | | | 1.020 | 1.363 |
| CA···HSO(S3) | B3LYP | 1.963 | 2.313 | 170 | 137 | | | 1.015 | 1.375 |
| | B3PW91 | 1.958 | 2.308 | 170 | 138 | | | 1.014 | 1.374 |
| | MP2 | 1.867 | 2.321 | 169 | 130 | | | 1.018 | 1.362 |
| CA···HOS(S1) | B3LYP | 2.265 | 1.661 | 168 | 170 | 0.989 | 0.999 | | |
| | B3PW91 | 2.201 | 1.619 | 168 | 170 | 0.992 | 1.003 | | |
| | MP2 | 2.266 | 1.678 | 169 | 170 | 0.982 | 0.990 | | |
| CA···HOS(S2) | B3LYP | 2.545 | 1.697 | 152 | 174 | 0.994 | 1.016 | | |
| | B3PW91 | 2.480 | 1.665 | 152 | 175 | | 0.996 | 1.017 | |
| | MP2 | | | | | | | | |
| CA···HOS(S3) | B3LYP | 2.560 | 1.829 | 160 | 172 | | 0.980 | 1.014 | |
| | B3PW91 | 2.510 | 1.811 | 161 | 172 | | 0.980 | 1.015 | |
| | MP2 | 2.563 | 1.833 | 161 | 171 | | 0.975 | 1.012 | |

[a] HB1 and HB2 are mentioned in H-bond key in Fig. 1

[b] O–Ha = OH bond of carbamic acid in complexes

[c] O–Hb = OH bond of $HO_2$, HSO and HOS in complexes

[d] Monomer O–H bond lengths are labeled on in Fig. 1

**Table 2** Energetic analysis (kJ $mol^{-1}$) computed at various levels of theories and basis sets for H-bonded complexes. *CBS* Complete basis set, *BSSE* basis set superposition error, *EDA* energy decomposition analysis

| Species | B3LYP | B3PW91 | $MP2_{(original)}$ | $MP2_{(CBS)}$ | $BSSE_{MP2(CBS)}$ | $\Delta E^{CP}_{MP2(CBS)}$ | EDA |
|---|---|---|---|---|---|---|---|
| CA···HO2(S1) | −71.10 | −69.57 | −67.30 | −79.01 | 4.13 | −74.87 | −71.67 |
| CA···HO2(S2) | −61.31 | −58.45 | −58.00 | −66.30 | 3.46 | −62.84 | −57.99 |
| CA···HO2(S3) | −39.62 | −35.52 | −39.61 | −42.00 | 3.62 | −38.39 | −35.10 |
| CA···HSO(S1) | −48.91 | −45.95 | −65.80 | −61.10 | 3.82 | −57.28 | −66.53 |
| CA···HSO(S2) | −40.40 | −37.13 | −52.61 | −50.11 | 3.92 | −46.08 | −53.01 |
| CA···HSO(S3) | −28.41 | −24.32 | −42.92 | −36.70 | 3.27 | −33.43 | −38.19 |
| CA···HOS(S1) | −59.33 | −56.04 | −58.51 | −71.83 | 4.53 | −67.27 | −61.11 |
| CA···HOS(S2) | −50.91 | −46.69 | −50.83 | −61.61 | 3.68 | −57.92 | −51.99 |
| CA···HOS(S3) | −32.20 | −26.23 | −36.20 | −39.80 | 3.73 | −36.07 | −31.29 |

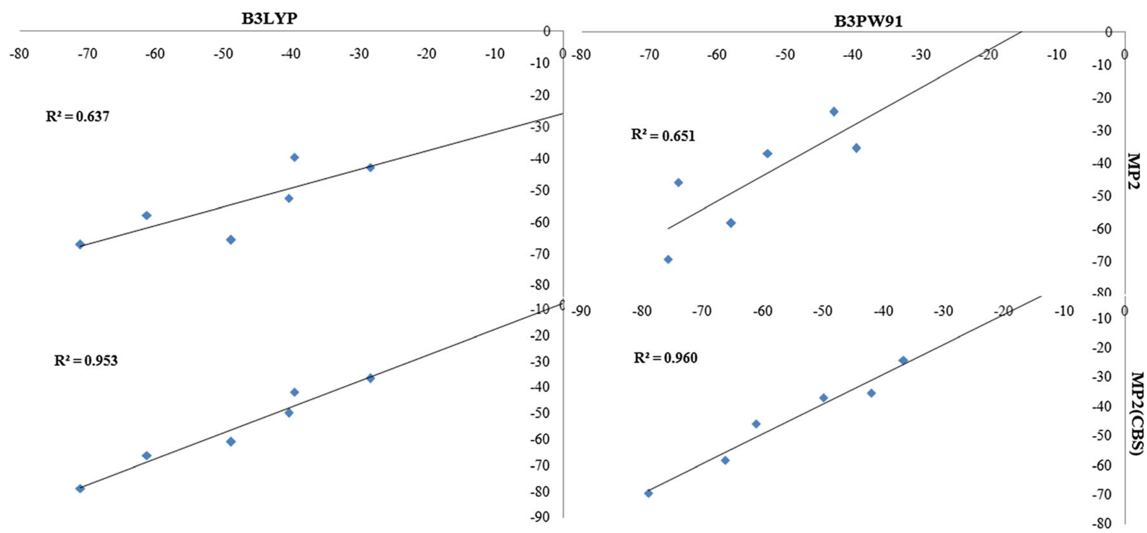


**Fig. 4** Correlation between $\Delta E_{int}$ values obtained by the B3LYP/MP2, B3LYP/ MP2(CBS), B3PW91/MP2 and B3PW91/MP2 [complete basis set (CBS)] theories

CA···HSO(S-2): N–H···O, S–H···O are 1.949, 2.044 Å; in CA···OH(S-3): O···H–O, H–O···H are 2.048, 1.796 Å; in CA···HSO: O···H–N, S–H···O are 1.963, 2.313 Å; in CA···HOS(S-1): O···H–O, O–H···S are 1.661, 2.265 Å; in CA···HOS(S-2): O–H···O, S···H–N are 1.697, 2.545 Å; and in CA···HOS(S-3): O–H···O, S···H–N are 1.829, 2.560 Å, respectively. From these HB distances, it is evident that O–H···O and O···H–O are stronger HBs compared to N–H···O, S–H···O, O–H···S and N–H···S HBs. The intermolecular HB angles θ(HB) for all complexes are listed in Table 1. The ideal angle of an HB complex is considered to be 180°. Note that the deviation from 180° is less in O–H···O and O···H–O H-bond (tilted up to 5–11°) as compared to N–H···O and S–H···O. The O–H and N–H stretching frequencies (Table S1)

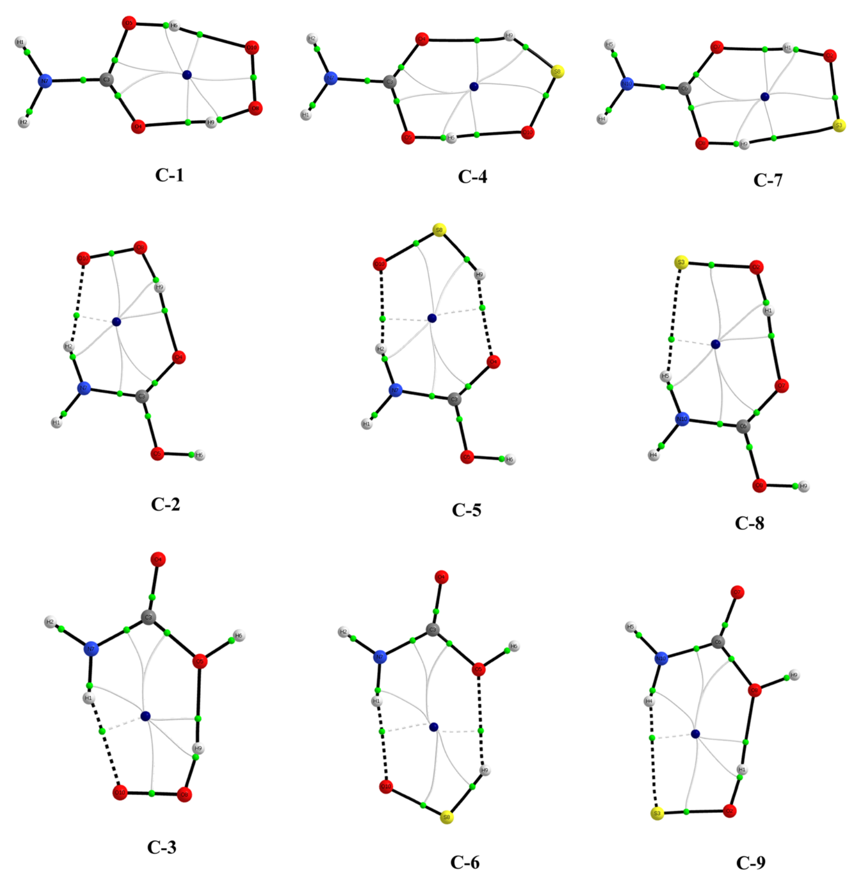


**Fig. 5** Molecular graphs and bond paths of OSHB complexes of CA. *Green balls* Bond critical points (BCP), *dark blue balls* ring critical points (RCP)

**Table 3** Quantum theory of atoms in molecules (QTAIM) parameters for HB complexes evaluated at various level of theories and 6–311++G** basis set. Values shown are B3LYP (MP2)

| | $\rho$ | | $\nabla^2\rho$ | | H | |
|---|---|---|---|---|---|---|
| | X–H···Y | Y···H–X | X–H···Y | Y···H–X | X–H···Y | Y···H–X |
| CA···HO2(S1) | 0.0404 (0.0408) | 0.0589 (0.0573) | 0.1152 (0.1209) | 0.1482 (0.1523) | −0.0028 (−0.0035) | −0.0111 (−0.0112) |
| CA···HO2(S2) | 0.0224 (0.0203) | 0.0504 (0.0469) | 0.1209 (0.0702) | 0.1523 (0.1421) | 0.0017 (0.0015) | −0.0062 (−0.0054) |
| CA···HO2(S3) | 0.0344 (0.0324) | 0.0211 (0.0189) | 0.1200 (0.1188) | 0.0712 (0.0659) | 0.0018 (0.0016) | 0.0004 (0.0004) |
| CA···HSO(S1) | 0.038 (0.0474) | 0.0251 (0.0228) | 0.1233 (0.1473) | 0.0822 (0.0770) | −0.0013 (−0.0059) | 0.0021 (0.0018) |
| CA···HSO(S2) | 0.0249 (0.0298) | 0.0229 (0.0201) | 0.0901 (0.1097) | 0.0731 (0.0661) | 0.0021 (0.0016) | 0.0018 (0.0016) |
| CA···HSO(S3) | 0.0132 (0.0133) | 0.0234 (0.0287) | 0.0410 (0.0435) | 0.0873 (0.1087) | 0.0012 (0.0011) | 0.0023 (0.0013) |
| CA···HOS(S1) | 0.0274 (0.0266) | 0.0486 (0.0457) | 0.0487 (0.0519) | 0.1421 (0.1424) | −0.0018 (−0.0018) | 0.0057 (−0.005) |
| CA···HOS(S2) | 0.0154 (0.0149) | 0.0438 (0.0413) | 0.0373 (0.0388) | 0.1359 (0.1362) | 0.0011 (0.0011) | −0.0033 (−0.0029) |
| CA···HOS(S3) | 0.0309 (0.0303) | 0.0147 (0.0143) | 0.1131 (0.1146) | 0.0361 (0.0375) | 0.0013 (0.001) | 0.0012 (0.0011) |

imply red shifted HB while the S–H stretching indicate blue shifted HB in the corresponding complexes. A detailed discussion on stretching frequencies analysis is given in the Supporting Information. Interaction energies ($\Delta E_{int}$) were computed using the following equation;

$$\Delta E_{int} = E_{Complex} - \left(E_{Monomer(A)} + E_{Monomer(B)}\right) \quad (6)$$

where $E_{Complex}$ is the total complex energy, and $E_{Monomer(A)}$ and $E_{Monomer(B)}$ are the total energies of monomers A and B.

For the H-bonded complexes, $\Delta E_{int}$ were computed with the B-3LYP, B3PW91 and MP-2 method using the 6-311++G (d,p) basis-set. BSSE was applied to correct the $\Delta E_{int}$ values using the CP method [33]. The values of $\Delta E_{int}$, $\Delta E_{int}^{CP}$ and BSSE are given in Table 2. The summarized values reflect that the BSSE values for the B3LYP and B3PW91 methods are consistent with each other, but MP2 results are not as good as they should be: the BSSE values are huge. The BSSE results with the B3PW91 are, of course, expected to be similar to those obtained with B3LYP, as triple-zeta with a couple of polarization functions and diffuse functions is close enough to saturation for DFT-methods. The 6-311++G (d,p) should give as good a DFT as possible, but its performance with MP2 is not better. Apparently, the Pople basis sets (6-31G, 6-311G, etc.) converge to the complete-basis-set limit slower than other schemes. Therefore, to minimize BSSE errors, we

**Table 4** Stabilization energies ($E^{(2)}$ kcal mol$^{-1}$) for H-bonded complexes at various level of theories. *NBO* Natural bond orbital

| Complex | Donor (NBO) | Acceptor (NBO) | $E^{(2)}$ | | |
|---|---|---|---|---|---|
| | | | B3PW91 | B3LYP | MP2 |
| CA···HO2(S1) | LP (2) O4 | σ*(1) O8 - H9 | 17.44 | 14.56 | 15.58 |
| | LP (2) O10 | σ*(1) O5 - H 6 | 13.77 | 11.4 | 14.68 |
| CA···HSO(S1) | LP (2) O4 | σ*(1) S8 - H9 | 3.49 | 2.71 | 1.57 |
| | LP (2) O10 | σ*(1) O5 - H 6 | 9.31 | 8.15 | 13.02 |
| CA···HO2(S2) | LP (2) O4 | σ*(1) O8 - H9 | 12.35 | 10.91 | 10.52 |
| | LP (2) O10 | σ*(1) H2 - N7 | 4.82 | 4.26 | 4.09 |
| CA···HSO(S2) | LP (2) O4 | σ*(1) S8 - H9 | 3.32 | 2.76 | 1.56 |
| | LP (2) O10 | σ*(1) H2 - N7 | 4.05 | 3.71 | 4.37 |
| CA···HO2(S3) | LP (1) O5 | σ*(1) O8 - H9 | 6.79 | 6.5 | 5.88 |
| | LP (2) O10 | σ*(1) H1 - N7 | 4.30 | 4.06 | 3.82 |
| CA···HSO(S3) | LP (1) O5 | σ*(1) S8 - H 9 | 0.98 | 0.96 | 0.73 |
| | LP (2) O10 | σ*(1) H1 - N7 | 3.19 | 3.12 | 3.57 |
| CA···HOS(S1) | LP(2)O7 | σ*(1) H3 – O2 | 11.56 | 9.29 | 8.96 |
| | LP(2)S3 | σ*(1) H9 – O8 | 13.28 | 10.59 | 13.96 |
| CA···HOS(S2) | LP(2)O7 | σ*(1) H3 – O2 | 9.23 | 7.82 | 7.59 |
| | LP(2)S3 | σ*(1) H5 – N10 | 4.82 | 3.79 | 4.62 |
| CA···HOS(S3) | LP(2)O8 | σ*(1) H3 – O2 | 5.54 | 5.15 | 4.76 |
| | LP(2)S3 | σ*(1) H4 – N10 | 4.36 | 3.64 | 4.44 |

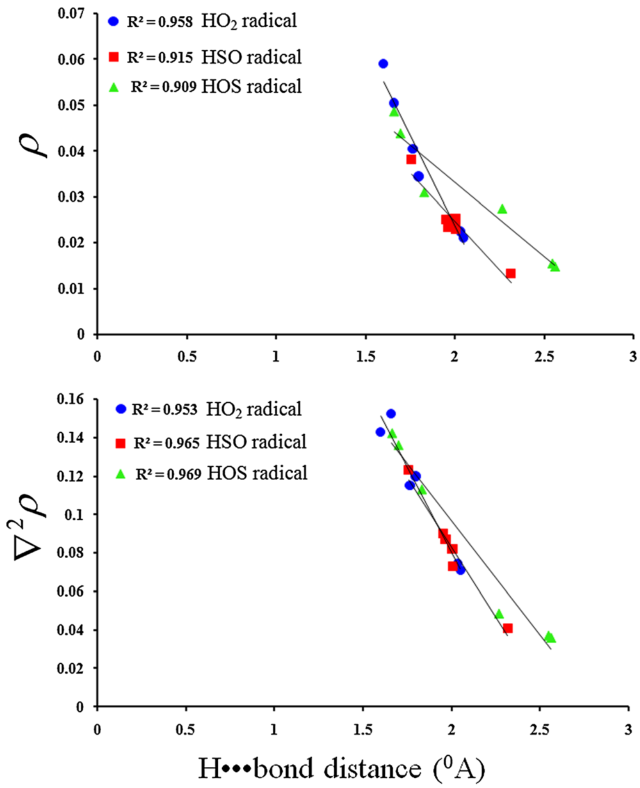


**Fig. 6** Correlation of electron density ($\rho$) and its Laplacian ($\nabla^2\rho$) value with HB distances

employed the MP2/CBS extrapolation scheme of Trauhlar [34] employing aug-cc-pVDZ and aug-cc-pVTZ basis sets. From the MP2/CBS extrapolation, we analyzed the correlations between B3LYP and MP2, which found that the correlation coefficient $R$ has improved from 0.800 to 0.976 (which means that $R^2$ has improved significantly, from 0.638 to 0.953). The correlation results are shown in Fig. 4. The MP2/CBS results for BSSE are collected in Table 2, and are now comparable with those of B3LYP and B3PW91 as presented in Fig. S5.

The order of MP2/CBS $-\Delta E_{int}^{CP}$ kj mol$^{-1}$ for intermolecular complexes is: CA⋯$HO_2$(S-1) > CA⋯HOS(S-1) > CA⋯HSO(S-1) > CA⋯HOS(S-2) > CA-$HO_2$(S-2) > CA⋯HSO(S-2) > CA⋯$HO_2$(S-3) > CA⋯HOS(S-3) > CA⋯HSO(S-3). Generally, the larger the negative $\Delta E_{int}$ value, the stronger the HB complex. Thus, for all the methods used, the strongest H-bonds are those where the carboxylic acid C=O of CA is an H-acceptor, and H-bonds with S–H and N–H are weaker than those of O–H.

## Bader's AIM analysis

The bond critical points (BCPs), ring critical points (RCPs) and molecular graphs of the OSHB complexes are shown in Fig. 5 (Fig. S2, S3). The values in Table 3 represents topological parameters, such as electron density, Laplacian and the corresponding total energy density values at BCPs. The presence of H-bonds based on the electron density paths and electron density values at the BCP, AIM analysis suggest specific criteria, and that is that $\rho$ and $\nabla^2\rho$ values are in the range of 0.002–0.035 and 0.024–0.139 a.u., respectively [40, 41]. These are the two basic quantitative criteria that are mostly applied to describe the H-bond strength. The H-bond is considered stronger if the charge density is larger. Table 4 indicates that the electron density ($\rho$) and Laplacian ($\nabla^2\rho$) values for the H-bonds of N–H ($\rho = 0.0203$–$0.0298$, $\nabla^2\rho = 0.0702$–$0.1097$) and S–H ($\rho = 0.0132$–$0.0251$, $\nabla^2\rho = 0.0401$–$0.0822$) are in the suggested range, while for the O–H (0.034–0.0589

**Fig. 7** Electron density difference (EDS) maps of complexes. The *blue* and *red regions* represent the increased and depleted electron density, respectively, plotted at isodensity contours 0.0008 electron per Bohr$^3$

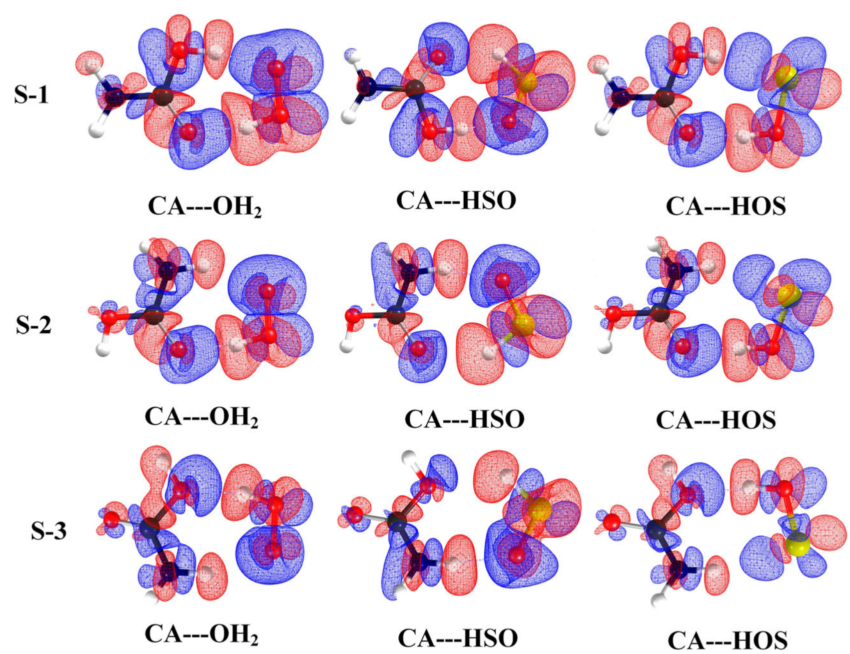

and 0.1152–0.1482 a.u.) they exceed the range proposed by Koch and Popelier [40, 41]. This shows that the O–H intermolecular HB is quite stronger.

From the analysis of $\rho$ and $\nabla^2\rho$ values in Table 4, it is clear that, in all three sites of CA, S-1 is more favorable for HB then S-2 and S-3. The strength of HBs is in the order CA···$HO_2$(S-1) > CA···$HO_2$(S-2) > CA···HOS(S-1) > CA···$HO_2$(S-2) > CA···HSO(S-1) > CA···HOS(S-3) > CA···HSO(S-2) > CA···HSO(S-3). These outcomes are in good agreement with the bond distances, energetic analysis

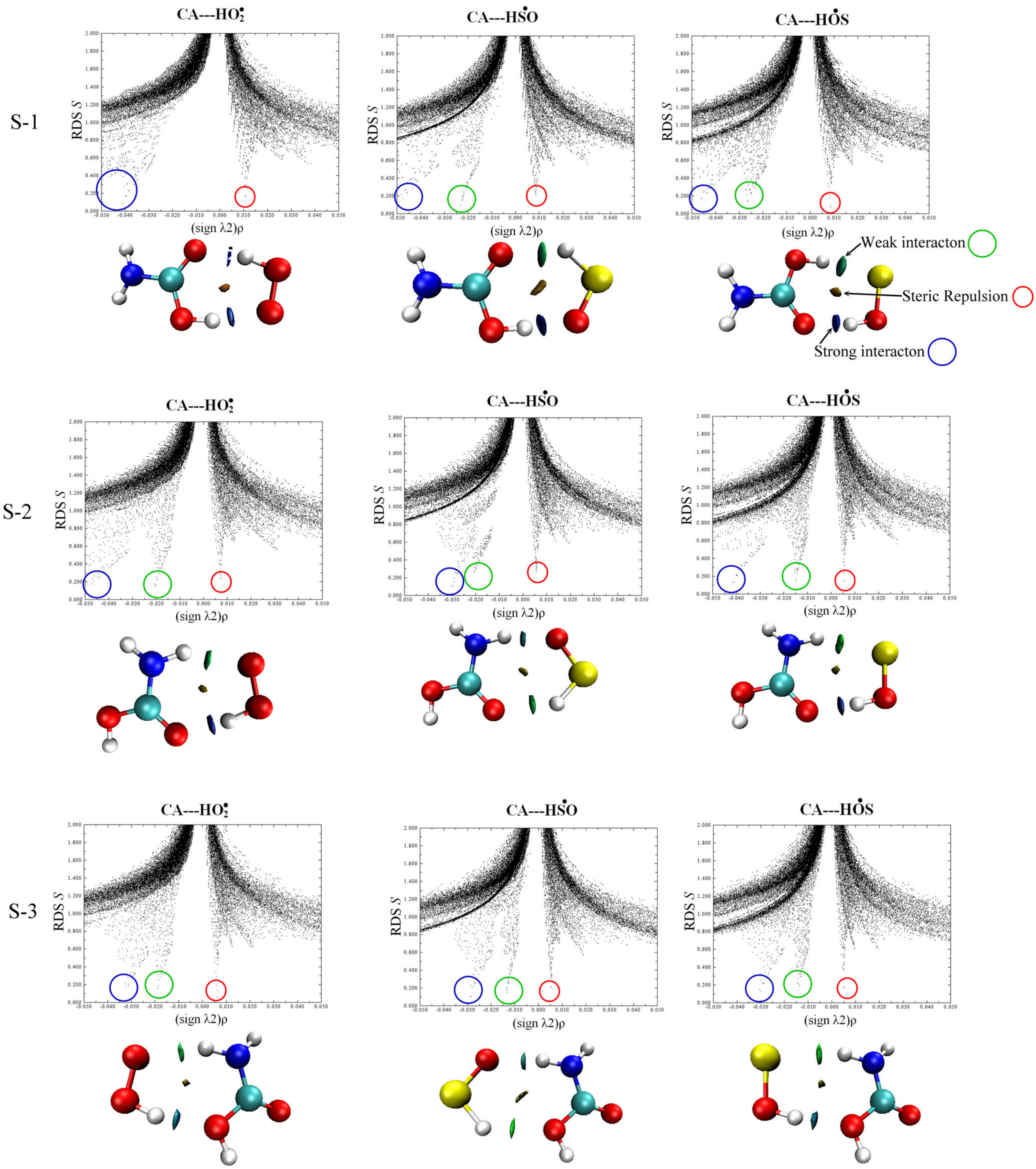


**Fig. 8** Reduced density gradient (RDG) vs sign ($\lambda_2$)ρ and noncovalent interaction (NCI) for the complexes: *blue*, *green* and *red circles* shows stronger, weak and repulsive interactions, respectively

and frequency analysis as discussed above. The correlation of $\rho$ and $\nabla^2\rho$ with bond lengths is presented in Fig. 6. The correlation plots indicate that there is inverse relationship between bond lengths and $\rho$ and $\nabla^2\rho$; when the charge density increases, the overlapping of orbital occurs, due to which the distances decrease. The values for correlation coefficients of $\rho$ and $\nabla^2\rho$ with hydrogen bond distances are 0.958 and 0.953 for $HO_2$ radical, 0.915 and 0.965 for HSO radical, and 0.909 and 0.969 for HOS radical.

Total electronic energy density (*H*) is also very useful to characterize HB [42]. *H* is a combination of kinetic-energy-density (*G*) and potential-energy-density (V). We determined the total electronic energy density with the help of a given equation.

$$H = G + V \tag{7}$$

Greater negative values of *H*®) generally indicate stronger H-bond interaction with a partially covalent characteristic, while positive H values shows weak electrostatic interaction involved in the H-bond [42]. The *H* values listed in the Table 4 are consistent with the geometrical parameters and $\Delta E_{int}$ of the complexes, i.e., the O–H···O intermolecular HB is stronger than N–H···O and S–H···OH-bonds.

## Electron density shifts and electron localization function analysis

To explore the characteristics of OSHB interactions, we also computed the electron density shift (EDS) isosurface of the title complexes (Fig. 7). These EDSs were calculated by subtracting the electron densities of the monomers (unperturbed) from the density of the corresponding complex. The blue (positive) and red (negative) regions in the EDS plots correspond to the charge accumulation and depletion, respectively. The plots show that, for the studied complexes, the charge accumulation in between the O and H, S and H regions is large, which reveals the formation of intermolecular H-bonds. Due to the accumulation of charge on the oxygen atom and depletion on the hydrogen atom in O···H interactions, the O–H bond is elongated, which is consistent with the bond lengths analysis as discussed above. The EDS results are in good agreement with energetic and AIM analysis, i.e., where C=O acts as an acceptor, and has stronger interactions, and O–H make stronger H-bonds than S–H and N–H.

Figure S4 shows the electron localization function (ELF) for the studied intermolecular HB complexes. It can be seen that the lone pair (LP) electrons of O and S atom are directed towards the H in XH (X = O, S, N) which is consistent with the bond length and AIM analysis.

## Noncovalent interaction and reduced density gradient analysis

The 2D reduced density gradient (RDG) plots and 3D noncovalent interaction (NCI) plots of the studied complexes are depicted in Fig. 8. The blue, green and red circles on the 2D and 3D plots represent strong and weak NCIs and steric repulsion in these complexes, respectively. Two spikes are evident from the RDG plot, and the values of spikes are (sign $\lambda_2)\rho < 0$, which shows a strong interaction. The blue circled spike shows a stronger inter-molecular HB interaction for these complexes as compared to the green circled spike. This justifies the consistency of the results with the AIM and energetic analysis, which show stronger H-bond existence where the O atom act as a H acceptor; O–H group act as H donor values are in the range of −0.04 to −0.05 a.u. Similarly, for the S atom as acceptor and N–H and S–H as H donor the values are in the range of −0.01 to −0.03 a.u., respectively. The RDG and NCI results provide evidence that, on all sites of CA (S-1, S-2 and S-3), O···H–O intermolecular H-bonding is the strongest bond as compared to the O···H–N, O···H–S, S···H–O and S···H–N H-bonding.

## Natural bond orbital analysis

Natural bond orbital (NBO) analysis is a very convenient tool for the understanding the mechanism of donor-acceptor charge-delocalization, which takes place between the LP of the B and empty antibonding orbital of the $\sigma^*$ (A−H) in the H-bonded A–H···B system [23]. To investigate the strength of the orbital interaction and the phenomena of red- and blue-shifting and charge transfer in the OH, NH and SH H-bonding, we performed NBO-analysis at MP-2, B-3LYP and B3PW91 methods by employing 6-311++G (d,p) basis set. The values of second-order perturbation energy ($E^2$), are summarized in Table 4.

The $E^{(2)}$ values for O, (LP) → σ* (H–O) charge transfer for S1 in CA···$HO_2$ complexes range from 6.79 to

**Table 5** Energy decomposition analysis (EDA; kcal $mol^{-1}$) for all complexes computed at the MP2/aug-cc-pVDZ level of theory

| | ES | EX | REP | POL | DISP | Total E |
|---|---|---|---|---|---|---|
| CA···HO2(S1) | −30.91 | −41.6 | 78.96 | −17.3 | −6.29 | −17.13 |
| CA···HO2(S2) | −22.48 | −27.15 | 50.64 | −10.35 | −4.52 | −13.86 |
| CA···HSO(S1) | −20.68 | −31.11 | 57.55 | −12.45 | −9.21 | −15.9 |
| CA···HSO(S2) | −15.24 | −21.76 | 39.21 | −7.07 | −7.81 | −12.67 |
| CA···HO2(S3) | −13.34 | −17.38 | 32.19 | −5.57 | −4.3 | −8.39 |
| CA···HSO(S3) | −10.58 | −15.88 | 28.8 | −4.54 | −6.93 | −9.13 |
| CA···HOS(S1) | −25.05 | −33.22 | 61.6 | −13.05 | −4.83 | −14.55 |
| CA···HOS(S2) | −19.89 | −24.67 | 45.3 | −9.05 | −4.07 | −12.38 |
| CA···HOS(S3) | −12.34 | −17.31 | 31.6 | −5.29 | −4.11 | −7.45 |

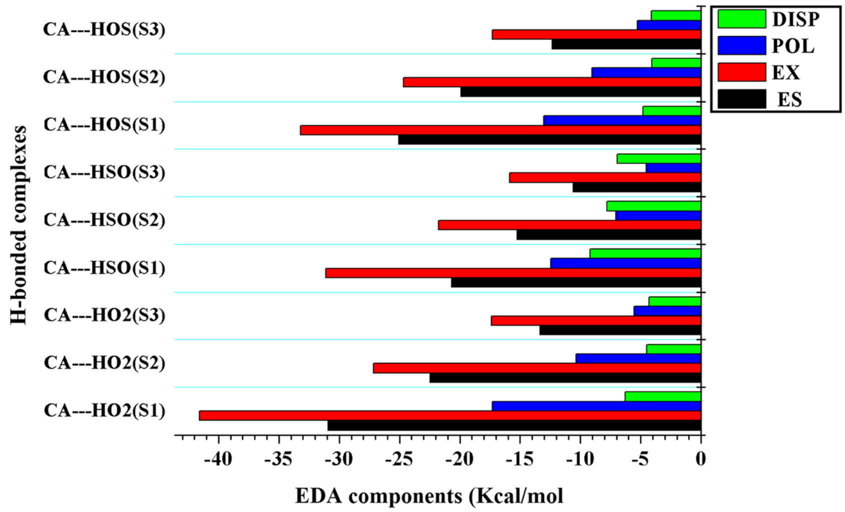


**Fig. 9** Contribution of various energy components (obtained from EDA) in the OSHB complexes

17.44 kcal mol$^{-1}$ for HB1 and from 4.30 to 13.77 kcal mol$^{-1}$ for HB2. While in the CA···HSO complexes for S1, S2 and S3, the stabilization-energy due to the O (LP) → σ* (H–S) orbital interaction ranges from 3.19 to 9.31 kcal mol$^{-1}$ for HB1 and from 0.98 to 3.49 kcal mol$^{-1}$ for HB2. In the CA···HOS complexes, the $E^{(2)}$ values for S1, S2 and S3 range from 4.36 to 13.28 kcal mol$^{-1}$ for HB1 and from 5.54 to 11.56 kcal mol$^{-1}$ for HB2. The values of $E^{(2)}$ strictly follow the order observed for the interaction energies, i.e., S1 of CA is favorable for H-bond formation with both types of radicals and $HO_2$ radical make the stronger H-bonded complexes then HSO and HOS radicals. These results are consistent with the $\rho$ and $\nabla^2\rho$ values, which indicate that stronger overlapping of orbitals is related to stronger intermolecular HB.

The NBO analysis results are also in agreement with the results of structural, energetic and AIM analysis, that is, O–H···O and O···H–O are stronger H-bonds than the others, and S-1 is a more favorable HB site.

## Application of EDA

To better understand the nature of the OSHB interactions studied here, the interaction energies were disintegrated into five components, including electrostatic (ES), exchange (EX), repulsion (REP), polarization (POL) and dispersion (DISP). Table 5 summarizes the results of these components. These results prove that, for all the complexes considered, the EX term has the larger values (−17.38 to −41.6 kcal mol$^{-1}$ for CA···HO2 complexes, −15.88 to −31.11 kcal mol$^{-1}$ for CA···HSO complexes and − 17.31 to −33.22 kcal mol$^{-1}$ for CA···HOS complexes, respectively) than other components, which indicates greater overlapping of molecular orbital and suggests stronger orbital interaction in the complexes. After EX, the magnitude of the ES term is larger than those of POL and DISP. The DISP contribution to HB is smaller compared to other components. A comparative plot drawn for the four attractive components (ES, EX, POL and DISP) is represented in Fig. 9. The plot shows the major contribution of EX and ES components in the OSHB complexes. Figure 10 show the correlation plot between EDA and the counterpoise total interaction energy, which are in good agreement ($R^2$ = 0.833). To compare the results of $E^{(2)}$ with the results of EDA indicates that ES and EX terms of EDA increases quickly with $E^{(2)}$ than POL and DISP terms which provide evidences that ES and EX are contributing more for charge transfer.

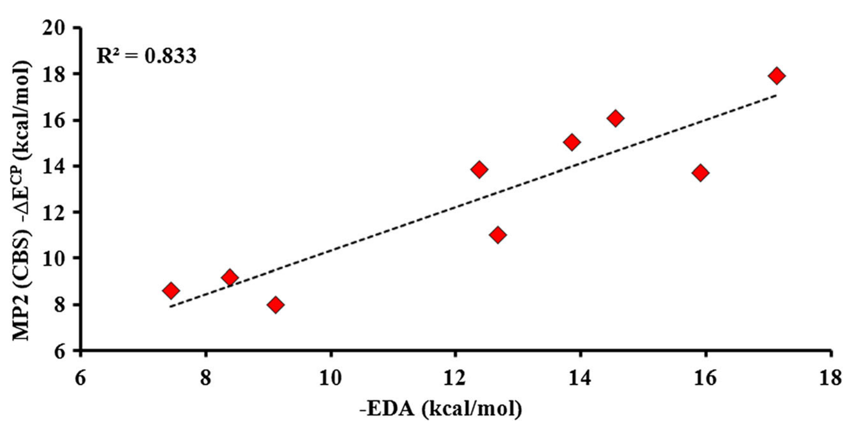


**Fig. 10** Correlation of MP2(CBS) $\Delta E^{CP}$ (kcal mol$^{-1}$) and EDA (kcal mol$^{-1}$)

## Conclusions

The OSHB interactions formed between the CA and $HO_2$, HSO or HOS radicals were investigated using MP2, B3PW91 and B3LYP computational methods. It was found that these radicals are attached to three different sites (S-1, S-2, S-3) of CA. Geometry optimization revealed that all the complexes consist of seven-membered rings. From the structural parameters and stretching frequencies analysis, it was observed that OH, NH bonds accompany a red shift, while the SH bond shows a blue shift. OH···O H-bonds are comparatively stronger than NH···O, SH···O, OH···S and NH···S H-bonds. The counterpoise corrected energies of B3LYP and B3PW91 and MP2/CBS interaction energies showed that H-bonded complexes of site-1(S-1) are more stable. The electron density $\rho$ and corresponding Laplacian $\nabla^2\rho$ were also computed using the AIM theory, and are in good agreement with structural and energetic analysis that OH···O H-bonds are stronger than NH···O, SH···O, OH···S and NH···S H-bonds. These results were further supported by NCI/RDG analysis. NBO analysis results coincide with those of structural, energetic and AIM analysis, that OH···O is a stronger hydrogen bond than the others, and S-1 is a more favorable site for HB, having higher stabilization energies ($E^{(2)}$)values. EDA analysis indicated that exchange energy makes a larger contribution in the OSHB complexes of CA, which provides the evidence for the larger overlap of orbitals in these systems.

**Acknowledgments** We acknowledge the financial support from the Higher Education Commission of Pakistan (HEC), Project No. 20-3959/NRPU/R&D/HEC2014/234.

## References

1. Daniel S, Lisa KW, Dwayne EH (2012) Tropospheric OH and $HO_2$ radicals: field measurements and model comparisons. Chem Soc Rev 41:6348–6404
2. Sasho G, Rafal S, Stephane B, Davide V (2015) Environmental implications of hydroxyl radicals (•OH). Chem Rev 115(24): 13051–13092
3. Javier G, Miquel TS, Josep MA (2010) The reactions of $SO_3$ with $HO_2$ radical and $H_2O$—$HO_2$ radical complex. Theoretical study on the atmospheric formation of $HSO_5$ and $H_2SO_4$. Phys Chem Chem Phys 12:2116–2125
4. Ignacio PJ, Luis C (2008) Theoretical study of the electronic and hyperfine structures of the HSO and SOH radicals. Theochem 855: 27–33
5. Takashi Y, Akihiro W, Yoshihiro S, Yasuki E (2009) Laser spectroscopy of the $A^2A$—$X^2A$ system for the HSO radical. J Mol Spectrosc 254:119–125
6. Ravishankara AR, Hancock G, Kawasaki M, Matsumi Y (1998) Photochemistry of ozone: surprises and recent lessons. Science 280(5360):60–61
7. Daniel RM, Giorgio ST, Clara AC, Trevor I, Martyn PC, Paul WS, Maria TBR, Dwayne EH (2018) Heterogeneous reaction of $HO_2$ with airborne $TiO_2$ particles and its implication for climate change mitigation strategies. Atmos Chem Phys 18:327–338
8. Ravi J, Tapan KG (2013) Hydrogen bonding interaction between $HO_2$ radical and selected organic acids, RCOOH (R= CH3, H, Cl and F). Chem Phys Lett 584:43–48
9. Spinks JWT, Woods RJ (1990) An introduction to radiation chemistry. Wiley, New York
10. Lelieveld J, Crutzen PJ (1990) Influences of cloud photochemical processes on tropospheric ozone. 343(6255):227
11. Ravishankara AR (1997) Heterogeneous and multiphase chemistry in the troposphere. Science 276(5315):1058–1065
12. DeMore WB, Sander SP, Golden DM, Hampson RF, Kurylo MJ, Howard CJ, Ravishankara AR, Kolb CE, Molina MJ (1997) Chemical kinetics and photochemical data for use in stratospheric modeling, JPL Publication 97–4, NASA, Washington, DC
13. Ralf S, Yana S (2010) Reversal of the relative stability of the isomeric radicals HSO and HOS upon hydration and their reactions with ozone. J Phys Chem A 114:4437–4445
14. Paul SM (2005) Gas-phase radical chemistry in the troposphere. Chem Soc Rev 34:376–395
15. Liuxie L, Shuang M, Quan L, Xiaolan W, Mingli Y, Laicai L (2017) Confinement of hydrogen and hydroxyl radicals in water cages: a density functional theory study. RSC Adv 7:14537
16. Aloisio S, Francisco JS (1998) Existence of a hydroperoxy and water ($HO_2$···$H_2O$) radical complex. J Phys Chem A 102:1899
17. Miller CE, Francisco JS (2001) The formation of a surprisingly stable $HO_2$···$H_2$SO4 complex. J Am Chem Soc 123(42):10387–10388
18. Solimannejad M, Azimi G, Pejov L (2004) The HOO–$SO_3$ radical complex: *ab Initio* and density-functional study. J Chem Phys Lett 391:201
19. Bil A, Latajka Z (2004) The hydroperoxy radical and its closed-shell analogues: *ab initio* investigations. Chem Phys Lett 388:158
20. Bil A, Latajka Z (2006) The Hydroperoxy radical as a hydrogen bond acceptor. HOO···HCl complexes-*ab initio* study. J Comput Chem 27:287
21. Solimannejad M, Nielsen CJ, Scheiner S (2008) Complexes pairing aliphatic amines with hydroxyl and hydroperoxyl radicals: a computational study. Chem Phys Lett 466:136
22. Solimannejad M, Scheiner S (2006) Stabilities and properties of complexes pairing hydroperoxyl radical with Monohalo Methanes. J Phys Chem A 110:5948
23. Yang Y, Liu Y (2010) Hydrogen bond of radicals: interaction of HNO with HCO, HNO, and HOO. Int J Quantum Chem 110:1264–1272
24. Arce VB, Gargarello RM, Ortega F, Romañano V, Mizrahi M, López JMR, Cobos CJ, Airoldi C, Bernardelli C, Donati ER, Mártire DO (2015) EXAFS and DFT study of the cadmium and lead adsorption on modified silica nanoparticles. Spectrochim Acta A Mol Biomol Spectrosc 151:156–163
25. Jing X, Siddarth S, Michael JJ (2014) $CO_2$ adsorption thermodynamics over N-substituted/grafted graphenes: a DFT study. Langmuir 30:1837–1844
26. Yuzhong N, Jinyun Y, Rongjun Q, Yanhong G, Na D, Hou C, Changmei S, Wenxiang W (2016) Synthesis of silica-gel-supported sulfur-capped PAMAM dendrimers for efficient hg(II) adsorption: experimental and DFT study. Ind Eng Chem Res 55: 3679–3688
27. Liu AH, Ma R, Song C, Yang ZZ, Yu A, Cai Y, He LN, Zhao YN, Yu B, Song QW (2012) Equimolar $CO_2$ capture by N-substituted amino acid salts and subsequent conversion. Angew Chem Int Ed 51:11306–11310
28. Frisch MJ, Trucks GW, Schlegel HB, Scuseria GE, Robb MA, Cheeseman JR, Scalmani G, Barone V, Mennucci B, Petersson GA et al (2009) Gaussian 09, revision C.01. Gaussian, Inc., Wallingford

29. Perdew JP, Burke K, Wang Y (1996) Generalized gradient approximation for the exchange-correlation hole of a many-electron system. Phys Rev B 54:16533–16539
30. Becke AD (1993) Density-functional thermochemistry. III. The role of exact exchange. J Phys Condens Matter 98:5648
31. Moller C, Plesset MS (1943) Note on an approximation treatment for many-electron systems. Phys Rev 46:618
32. Krishnan R, Binkley JS, Seeger R, Pople JA (1980) Self-consistent molecular orbital methods. XX. A basis set for correlated wave functions. J Chem Phys 72:650–654
33. Boys SF, Bernardi F (1970) The calculation of small molecular interactions by the differences of separate total energies. Some procedures with reduced errors. Mol Phys 19:553
34. Truhlar DG (1998) Basis-set extrapolation. Chem Phys Lett 294: 45–48
35. Zhao Y, Truhlar DG (2005) Infinite-basis calculations of binding energies for the hydrogen bonded and stacked tetramers of formic acid and formamide and their use for validation of hybrid DFT and ab initio methods. J Phys Chem A 109:6624–6627
36. Su P, Jiang Z, Chen Z, Wu W (2014) Energy decomposition scheme based on the generalized Kohn−Sham scheme. J Phys Chem A 118: 2531–2542
37. Yu F (2013) Intermolecular interactions of formic acid with benzene: energy decomposition analyses with ab initio MP2 and double hybrid density functional computations. Int J Quantum Chem 113:2355–2360
38. Schmidt MW, Baldridge KK, Boatz JA, Elbert ST, Gordon MS, Jensen JH, Koseki S, Matsunaga N, Nguyen KA, Su S et al (1993) General atomic and molecular electronic structure system. J Comput Chem 14:1347–1363
39. Gordon MS, Schmidt MW (2005) Advances in electronic structure theory: GAMESS a decade later. In: Dykstra CE, Frenking G, Kim KS, Scuseria GE (eds) Theory and applications of computational chemistry: the first forty years. Amsterdam, Elsevier, pp 1167–1189
40. Gilli P, Bertolasi V, Ferretti V, Gilli G (1994) Covalent nature of the strong Homonuclear hydrogen bond. Study of the O–H–O system by crystal structure correlation methods. J Am Chem Soc 116:909–915
41. Koch U, Popelier PLA (1995) Characterization of C-H-O hydrogen bonds on the basis of the charge density. J Phys Chem 99:9747–9754
42. Varadwaj PR, Varadwaj A, Jin BY (2014) Halogen bonding interaction of chloromethane with several nitrogen donating molecules: addressing the nature of the chlorine surface σ-hole. Phys Chem Chem Phys 16:19573